NMR Structural Analysis of an Analog of an Intermediate Formed in the Rate-Determining Step of One Pathway in the Oxidative Folding of Bovine Pancreatic Ribonuclease A: Automated Analysis of ^{1}H, ^{13}C, and ^{15}N Resonance Assignments for Wild-Type and [C65S, C72S] Mutant Forms†

Sakurako Shimotakahara,‡,§ Carlos B. Ríos,‡ John H. Laity,§ Diane E. Zimmerman,‡ Harold A. Scheraga,*,§ and Gaetano T. Montelione*,‡

Center for Advanced Biotechnology and Medicine and Department of Molecular Biology and Biochemistry, Rutgers University, Piscataway, New Jersey 08854-5638, and Baker Laboratory of Chemistry, Cornell University, Ithaca, New York 14853-1301

Received December 10, 1996; Revised Manuscript Received March 17, 1997⊗

ABSTRACT: A three-disulfide intermediate, des-[65−72] RNase A, lacking the disulfide bond between Cys65 and Cys72, is formed in one of the rate-determining steps of the oxidative regeneration pathways of bovine pancreatic ribonuclease A (RNase A). An analog of this intermediate, [C65S, C72S] RNase A, has been characterized in terms of structure and thermodynamic stability. Triple-resonance NMR data were analyzed using an automated assignment program, AUTOASSIGN. Nearly all backbone ^{1}H, ^{13}C, and ^{15}N resonances and most side-chain $^{13}C^{\beta}$ resonances of both wild-type (wt) and [C65S, C72S] RNase A were assigned unambiguously. Analysis of NOE, $^{13}C^{\alpha}$ chemical shift, and $^{3}J(H^{N}-H^{\alpha})$ scalar coupling data indicates that the regular backbone structure of the major form of [C65S, C72S] RNase A is very similar to that of the major form of wt RNase A, although small structural differences are indicated in the mutation site and in spatially adjacent β-sheet structures comprising the hydrophobic core. Thermodynamic analysis demonstrates that [C65S, C72S] RNase A (T_m of 38.5 °C) is significantly less stable than wt RNase A (T_m of 55.5 °C) at pH 4.6. Although the structural comparison of wt RNase A and this analog of an oxidative folding intermediate indicates only localized effects around the Cys65 and Cys72 sites, these thermodynamic measurements indicate that formation of the fourth disulfide bond, Cys65−Cys72, on this oxidative folding pathway results in global stabilization of the native chain fold. This conclusion is supported by comparisons of amide $^{1}H/^{2}H$ exchange rates which are significantly faster throughout the entire structure of [C65S, C72S] RNase A than in wt RNase A. More generally, our study indicates that the C65−C72 disulfide bond of RNase A contributes significantly in stabilizing the structure of the hydrophobic core of the native protein. Formation of this disulfide bond in the final step of this oxidative folding pathway provides significant stabilization of the native-like structure that is present in the corresponding three-disulfide folding intermediate.

Structural analysis of folding and unfolding intermediates can provide crucial information needed for solving the protein folding problem. One of the central issues in the field of protein folding involves characterization of the number of pathways in oxidative folding of disulfide-containing proteins through which any particular protein folds (Konishi & Scheraga, 1980a,b; Konishi *et al.*, 1981, 1982a−c; Scheraga *et al.*, 1984, 1987; Creighton, 1988a). One view has been the "single-pathway" mechanism (Privalov, 1979; Creighton, 1988b), in which proteins fold through one unique rate-determining step. However, it is not yet clear that the single-pathway mechanism is applicable to proteins in general, particularly for proteins with complex folding kinetics. Recent studies of the oxidative folding mechanisms of bovine pancreatic ribonuclease A (RNase A)[1] indicate that, for this small protein, the single-pathway mechanism does not apply (Konishi *et al.*, 1981; Rothwarf & Scheraga, 1993a−d; Li *et al.*, 1995).

RNase A contains 124 amino acid residues and four disulfide bonds (Cys26−Cys84, Cys40−Cys95, Cys58−Cys110, and Cys65−Cys72). It unfolds upon reduction of its disulfide bonds, even in the absence of denaturants, which indicates that folding is coupled to disulfide bond formation.

† This work was supported by grants from the National Institutes of Health (GM-24893 to H.A.S. and GM-47014 to G.T.M.), the National Science Foundation (MCB-9407569 to G.T.M.), a National Science Foundation Young Investigator Award (MBC-9357526 to G.T.M.), the National Foundation for Cancer Research (to H.A.S.), and a Camille Dreyfus Teacher-Scholar Award (to G.T.M.). S.S. and J.H.L. were NIH trainees at Cornell University.

* Address correspondence to these authors. G.T.M.: phone, 908-235-5321; Fax, 908-235-4850; E-mail, guy@nmrlab.cabm.rutgers.edu. H.A.S.: phone, 607-255-4034; Fax, 607-254-4700; E-mail, has5@cornell.edu.

‡ Rutgers University.

§ Cornell University.

⊗ Abstract published in *Advance ACS Abstracts,* May 15, 1997.

[1] Abbreviations: 3D, three dimensional; AEMTS, (2-aminoethyl)-methanethiosulfonate; cCMP, cyclic cytidine monophosphate; CFIS, chain-folding initiation site; FPLC, fast performance liquid chromatography; MALDI-TOF, matrix-assisted laser desorption ion time of flight; GS, generic amino acid spin system with no site-specific assignment; $^{1}H/^{2}H$ exchange, amide hydrogen/deuterium exchange; HSQC, heteronuclear single-quantum coherence; NOESY, nuclear Overhauser effect spectroscopy; OD, optical density; PFG, pulsed-field gradient; pH*, uncorrected pH meter reading of a $^{2}H_2O$ protein solution; RNase A, bovine pancreatic ribonuclease A; [C65S, C72S] RNase A, an analog of the des-[65−72] RNase A oxidative folding intermediate with Cys65 and Cys72 replaced by serines; wt, wild type.

S0006-2960(96)03024-3 CCC: $14.00

Therefore, the folding process can be monitored through disulfide bond formation. Extensive studies of the thermodynamic stability, structure, and folding/unfolding kinetics of wild-type (wt) RNase A suggest that RNase A folds through multiple pathways (Konishi *et al.*, 1981; Rothwarf & Scheraga, 1993a−d; Li *et al.*, 1995). Specifically, two three-disulfide intermediates, des-[40−95] and des-[65−72] RNase A lacking the 40−95 and 65−72 disulfide bonds, respectively, are observed in the oxidative regeneration or reductive unfolding of RNase A (Li *et al.*, 1995). These two three-disulfide species are intermediates on different folding and unfolding pathways (Li *et al.*, 1995). Moreover, the formation of these two intermediates has been found to be the rate-determining step in each of these two different folding pathways (Li *et al.*, 1995).

It has been proposed that short-range interactions can dominate in the early stages of folding to form transient local structures that play a critical role in protein folding mechanisms (Matheson & Scheraga, 1978; Némethy & Scheraga, 1979; Montelione *et al*., 1984; Wright *et al.*, 1988; Baldwin, 1989; Montelione & Scheraga, 1989; Freund *et al.*, 1996). The presence of these chain-folding initiation structures (CFIS's) is thought to limit the conformational space accessible to the protein in the initial stages of the folding process, thereby directing subsequent folding events. Several studies have indicated the existence of possible CFIS's for wt RNase A (Matheson & Scheraga, 1978; Chavez & Scheraga, 1980; Montelione *et al.*, 1984; Oka *et al.*, 1984; Swadesh *et al.*, 1984; Montelione & Scheraga, 1989; Udgaonkar & Baldwin, 1990; Altmann & Scheraga, 1990; Buckler *et al.*, 1995; Dodge *et al.*, 1996; Xu *et al.*, 1996). In particular, the loop structure formed by the C65−C72 disulfide bond has been proposed as a possible CFIS (Némethy & Scheraga, 1979; Montelione & Scheraga, 1989; Altmann & Scheraga, 1990; Xu *et al.*, 1996). As reported by Xu *et al.* (1996), the isolation and characterization of single disulfide bond intermediates in the early stages of oxidative folding reveal that ∼40% of these intermediates involve a C65−C72 disulfide bond. This result is consistent with an earlier study of a short peptide corresponding to the terminally-blocked polypeptide segment Cys58−Cys72, in which the formation of the C65−C72 disulfide bond was found to be favored by local interactions over the C58−C65 or C58−C72 disulfides (Altmann & Scheraga, 1990). Xu *et al.* (1996) have suggested that the C65−C72 disulfide bond may be highly populated in the two- and three-disulfide intermediates along the folding pathway.

One method to study kinetic folding and unfolding intermediates involves the use of blocking reagents to modify free cysteine residues selectively. Although such thiol blocking can be rapid and efficient (Creighton, 1986; Rothwarf & Scheraga, 1991), these blocking groups may introduce undesirable side effects, including steric and/or electrostatic interactions with other parts of the protein. A previous NMR study of des-[65−72] RNase A (Talluri *et al.*, 1994), prepared by reacting the reduced Cys65 and Cys72 residues with the blocking reagent (2-aminoethyl)methanethiosulfonate (AEMTS) has suggested that the rate-determining step in the reductive unfolding pathway that includes des-[65−72] RNase A involves a *local* unfolding process. However, that NMR study was limited by (i) uncertainty regarding the effects of chemical modification on the local structure of this analog of a folding intermediate, (ii) the low solubility of this chemically modified protein, and (iii) significant overlap of resonances in the homonuclear NMR spectra. To eliminate effects of charged blocking groups on the conformation of this three-disulfide species, we have prepared a mutant protein, [C65S, C72S] RNase A (Laity *et al.*, 1993), in which the Cys65 and Cys72 residues are replaced by serines. This mutant analog exhibits sufficient solubility for extensive NMR studies. To address the third issue, we have utilized heteronuclear 3D NMR experiments for determining resonance assignments and for carrying out structural analysis.

The primary goal of this study is to provide a better characterization of the locations and extents of structural distortions which result from removal of the Cys65−Cys72 disulfide bond in order to better define the structural differences between this three-disulfide folding intermediate and wt RNase A. To improve the efficiency and speed of the assignment procedure, an expert system, AUTOASSIGN (Zimmerman & Montelione, 1995; Zimmerman *et al.*, 1997), was used for automated analysis of triple-resonance spectra. In this paper, we present sequence-specific ^{1}H, ^{13}C, and ^{15}N backbone and $^{13}C^{\beta}$ resonance assignments for both wt and [C65S, C72S] RNase A, determined by triple-resonance NMR techniques and analyzed by AUTOASSIGN. These assignments provide the basis for analysis of NOEs, $^{3}J(H^{N}-H^{\alpha})$ coupling constants, and amide $^{1}H/^{2}H$ exchange rate data. Comparison of these data for wt and [C65S, C72S] RNase A demonstrates that the removal of the Cys65−Cys72 disulfide bond affects the chemical shifts of residues that are nearby in the three-dimensional structure and results in an increase in $^{1}H/^{2}H$ exchange rates for backbone amides located throughout the protein fold. Analysis of chemical shift, NOE, and scalar coupling data shows that the overall structures of wt and [C65S, C72S] RNase A are quite similar. Most importantly, our results reveal that small perturbations in local structure around the mutation sites have *global* effects on the stability of the RNase A chain fold; this effect on global stability arises in part from subtle alterations of β-sheet structures constituting the hydrophobic core of RNase A. These data demonstrate that formation of the fourth disulfide bond in des-[65−72] RNase A plays a crucial role in the folding mechanism by stabilizing the native-like RNase A structure that is already present in the corresponding three-disulfide folding intermediate.

MATERIALS AND METHODS

Sample Preparation. Uniformly ^{15}N-enriched [C65S, C72S] RNase A was expressed using plasmid pMMII[C65S, C72S] in *Escherichia coli* strain HMS174(DE3) and purified as described previously (Laity *et al.*, 1993). The pMMII-[C65S, C72S] vector was constructed by subcloning the gene 10 [C65S, C72S] RNase A gene from pSJII[C65S, C72S] (Laity *et al.*, 1993) into the pET21b expression plasmid (Novagen). Uniformly ^{13}C,^{15}N-enriched [C65S, C72S] RNase A was produced using plasmid pRM[C65S, C72S] in *E. coli* strain BL21(DE3). This expression plasmid was constructed by subcloning the [C65S, C72S] RNase A gene from pSJII-[C65S, C72S] into the *Msc*I/*Hin*dIII region of a pET22b vector (Novagen) as described by delCardayré *et al.* (1995). The required *Msc*I site was created by polymerase chain reaction (PCR) methods using a Perkin-Elmer Gene Amp PCR System 2400. Both ^{15}N- and ^{13}C,^{15}N-enriched wt

RNase A were expressed using plasmid pXBR-2 (delCardayré *et al.*, 1995) in *E. coli* strain BL21(DE3).

A single colony of BL21(DE3) *E. coli* was grown in liquid broth (LB) media on agar plates overnight and then inoculated into 15 mL of LB media containing 200 μg/mL ampicillin at 37 °C with constant shaking at 225 rpm. This cell culture was grown until it reached an OD_{600} of about 0.8. At this point, the cell suspension was centrifuged at 2500 rpm for 10 min, the supernatant was removed, and the cell pellet was used to inoculate 1 L of MJ minimal media (Jansson *et al.*, 1996) containing 2.5 g of $(^{15}NH_4)_2SO_4$, 3.0 g of glucose or [U-^{13}C] glucose (for ^{13}C,^{15}N enrichment only), trace elements, vitamin solutions, and 50 μg/mL ampicillin. This culture was incubated at 37 °C with shaking. When this growth culture reached an OD_{600} of 0.6−0.8, protein expression was induced by the addition of 5 mL of 0.1 M aqueous isopropyl β-D-thiogalactopyranoside. The culture was then incubated overnight with shaking at 37 °C. The isolation of expressed RNase A from inclusion bodies of the resulting cells and the sulfonation of the isolated protein were carried out as described previously (Laity *et al.*, 1993). The soluble sulfonated protein was then dialyzed exhaustively at 4 °C against 25 mM formic acid containing 3 M urea, pH 4.0, and the supernatant was exchanged into a folding buffer containing 0.1 M Tris and 3 mM EDTA, pH 8.2, using a Sepharose G-25M column (Pharmacia). The protein was then refolded and purified as described by Laity *et al.* (1993). All samples were analyzed by laser desorption mass spectroscopy (MALDI-TOF), N-terminal analysis, and amino acid analysis (Cornell Biotechnology Center) in order to ensure that the isotope enrichment was uniform (>97 ± 2%) and that the N-termini of the protein samples were correct. In addition, samples were analyzed by analytical cation-exchange chromatography using a Mono S (Pharmacia) or hydropore (Rainin) cation-exchange column and by analytical capillary electrophoresis (Cornell Biotechnology Center); the samples were found to contain <1% of chemical heterogeneity. Enzymatic activities of wt and [C65S, C72S] RNase A were assayed as described by Laity *et al.* (1993).

Thermal Transition Measurements. Samples for thermal transition measurements were prepared at ~12 μM protein concentration in 100 mM sodium acetate buffer at pH 4.6 ± 0.05. Absorption measurements were made at 287 nm using a modified Cary model 14 spectrophotometer with a 10.0 cm path-length quartz cell (Hellma) jacketed in water for temperature regulation, as described elsewhere (Laity *et al.*, 1993). Approximately 10 min was allowed for thermal equilibration at each temperature. All thermal transitions were observed to be >95% reversible. Analysis of thermodynamic parameters from these data was carried out using standard methods (Pace *et al.*, 1989).

NMR Spectroscopy. NMR samples of both wt and [C65S, C72S] RNase A were prepared by dissolving the lyophilized protein in H_2O containing 10% ^2H_2O, at pH* 4.6. This pH value was chosen so that the structural analysis of [C65S, C72S] RNase A could be compared with that reported for des-[65−72] RNase A by Talluri *et al.* (1994). All NMR data were collected using 5 mm susceptibility-matched Shigemi NMR tubes. Protein concentrations were 2.7 mM for the samples of uniformly ^{15}N-enriched wt and [C65S, C72S] RNase A, 2.0 mM for ^{13}C,^{15}N-enriched wt RNase A, and 3.0 mM for ^{13}C,^{15}N-enriched [C65S, C72S] RNase A. Samples were also analyzed by laser desorption mass spectroscopy, Mono S (Pharmacia) or hydropore (Rainin) cation-exchange chromatography, and analytical capillary electrophoresis, *after* the NMR experiments were complete in order to ensure that no chemical degradation or deamidation occurred during the NMR data collection.

All heteronuclear NMR spectra were recorded on a Varian Unity 500 NMR spectrometer system equipped with three full channels and a computer-controlled fourth frequency synthesizer for carbonyl decoupling. Homonuclear NOESY spectra were recorded on a Varian Unity Plus 600 NMR spectrometer system. In all spectra, quadrature detection was carried out in indirect dimensions either using the States−TPPI method (Marion *et al.*, 1989) or by combining n- and p-spectra (Nagayama, 1986; Kay et al., 1992) selected with pulsed-field gradients (PFGs). All NMR spectra were processed with the Varian VNMR software package.

2D NOESY spectra (Jeener *et al.*, 1979; Kumar *et al.*, 1980) were recorded using 512 complex points and a spectral width of 17 000 Hz in the t_1 dimension and 4096 complex points and a spectral width of 8000 Hz in the t_2 dimension. 3D ^{15}N-edited PFG NOESY-HSQC spectra [based on Driscoll *et al.* (1990); pulse sequence shown in supplementary Figure S1; see Supporting Information] were recorded using 150 complex points and a spectral width of 6300 Hz in t_1, 64 complex points and a spectral width of 2500 Hz in t_2, and 1024 complex points and a spectral width of 3500 Hz in t_3 (the offset was switched to the center of the amide proton region prior to acquisition). The NOESY mixing times were 80 ms for the 2D and ^{15}N-edited 3D spectra of both wt and [C65S, C72S] RNase A samples.

Pulsed-field gradient triple-resonance experiments were carried out using uniformly ^{13}C,^{15}N-enriched wt and [C65S, C72S] RNase A. For all triple-resonance experiments on wt RNase A, the spectral width in the t_3 dimension was 3400 Hz with the proton carrier set to the center of the amide proton region, while all data sets for [C65S, C72S] RNase A were recorded with a t_3 spectral width of 6900 Hz and the proton carrier set to the water resonance frequency in order to reduce the amplitude of spurious water echoes. For all triple-resonance experiments, the spectral width in the nitrogen (t_2) dimension was 2500 Hz.

3D PFG-HNCO data [based on Muhandiram and Kay (1994); pulse sequence shown in supplementary Figure S2] were acquired for wt and [C65S, C72S] RNase A using 50 × 50 × 512 and 40 × 40 × 1024 complex data points in the t_1, t_2, and t_3 dimensions, respectively, and four scans per t_1 or t_2 increment. The spectral widths in the carbon (t_1) dimension were 1500 and 2000 Hz for wt and [C65S, C72S] RNase A, respectively. For both samples, coherence transfer delays[2] were tuned to $\tau_a = 2.4$ ms and $\tau_b = 12$ ms. The constant-time evolution period was tuned to $\tau_f = 12$ ms.

3D PFG-HN(CA)CO spectra [based on Clubb *et al.* (1992); pulse sequence shown in supplementary Figure S3] were acquired for wt and [C65S, C72S] RNase A using 32 × 40 × 512 and 40 × 45 × 1024 complex data points in the t_1, t_2, and t_3 dimensions, respectively, and 16 scans per increment. The spectral width in the carbon (t_1) dimension was 2500 Hz. For both samples, coherence transfer delays

[2] τ_a, τ_b, τ_c, τ_d, τ_e, τ_f, T_c, and T_n are pulse sequence delays defined in Figures S1−S9 of the Supporting Information.

were tuned to $\tau_a = 2.3$ ms and $\tau_b = 2.4$ ms. The constant-time evolution period was tuned to $T_c = 10$ ms.

3D PFG-HNCA data [based on Muhandiram and Kay (1994); pulse sequence shown in supplementary Figure S4] were acquired for wt and [C65S, C72S] RNase A using 40 × 45 × 512 and 40 × 45 × 1024 complex data points in the t_1, t_2, and t_3 dimensions, respectively, and 16 or 12 scans per increment. For both samples, the spectral widths in the carbon (t_1) dimension were 6100 Hz, and coherence transfer delays were tuned to $\tau_a = 2.5$ ms and $\tau_b = 9.0$ ms. The constant-time evolution period was tuned to $\tau_f = 9.0$ ms.

3D PFG-CA(CO)NH data (Feng *et al.*, 1996; pulse sequence shown in supplementary Figure S5) were acquired for wt and [C65S, C72S] RNase A using 40 × 42 × 512 and 40 × 45 × 1024 complex data points in the t_1, t_2, and t_3 dimensions, respectively, and 16 or 12 scans per increment. The spectral widths in the carbon (t_1) dimension were 6000 and 6100 Hz for wt and [C65S, C72S] RNase A, respectively. For both samples, coherence transfer delays were tuned to $\tau_a = 1.5$ ms, $\tau_{a-foc} = 2.4$ ms, $\tau_b = 3.6$ ms, $\tau_c = 2.5$ ms, and $\tau_d = 14.0$ ms. The constant-time evolution periods were tuned to $T_c = 3.4$ ms and $T_n = 11.0$ ms.

Data for both 3D PFG-HA(CA)(CO)NH (Feng *et al.*, 1996; pulse sequence shown in supplementary Figure S6) and 3D PFG-HA(CA)NH experiments (Feng *et al.*, 1996; supplementary Figure S7) were acquired for wt and [C65S, C72S] RNase A using 30 × 45 × 512 and 40 × 45 × 1024 complex data points in the t_1, t_2, and t_3 dimensions, respectively, and 16 or 12 scans per increment. The spectral widths in the aliphatic proton (t_1) dimension were 4500 and 2500 Hz for wt and [C65S, C72S] RNase A, respectively. Coherence transfer delays were tuned to $\tau_a = 1.5$ ms, $\tau_{a-foc} = 2.4$ ms, $\tau_b = 3.6$ ms, $\tau_c = 2.5$ ms, and $\tau_d = 15.0$ ms. The constant-time evolution periods were tuned to $T_c = 3.4$ ms and $T_n = 11.0$ ms.

3D PFG-CBCA(CO)NH spectra (Grzesiek & Bax, 1992a; Ríos *et al.*, 1996; pulse sequence shown in supplementary Figure S8) were acquired for wt and [C65S, C72S] RNase A using 40 × 40 × 512 and 38 × 40 × 1024 complex data points in the t_1, t_2, and t_3 dimensions, respectively, and 16 scans per increment. The spectral width in the carbon (t_1) dimension was 10 000 Hz. For both samples, the coherence transfer delays were tuned to $\tau_a = 1.4$ ms, $\tau_{a-foc} = 2.1$ ms, $\tau_b = 4.5$ ms, $\tau_c = 2.7$ ms, $\tau_d = 14.0$ ms, and $\tau_e = 3.8$ ms. The constant-time evolution periods were tuned to $T_c = 3.3$ ms and $T_n = 11.0$ ms.

3D PFG-CBCANH spectra (Grzesiek & Bax, 1992b; pulse sequence shown in supplementary Figure S9) were acquired for wt and [C65S, C72S] RNase A using 32 × 40 × 512 and 48 × 45 × 1024 complex data points in the t_1, t_2, and t_3 dimensions, respectively, and 16−32 scans per increment. The spectral width in the carbon (t_1) dimension was 10 000 Hz. For both samples, the coherence transfer delays were tuned to $\tau_a = 1.5$ ms, $\tau_{a-foc} = 2.1$ ms, $\tau_c = 2.5$ ms, $\tau_d = 4.0$ ms, and $\tau_e = 3.8$ ms. The constant-time evolution periods were tuned to $T_c = 2.4$ ms and $T_n = 11.0$ ms.

For all spectra, Gaussian window functions were applied in all three dimensions, and linear prediction and zero filling were used to extend the time-domain data in the carbon (t_1) and/or nitrogen (t_2) dimension. The final size of the 3D matrix was 256 × 256 × 1024 for all spectra.

Amide proton exchange rates for wt and [C65S, C72S] RNase A were measured by dissolving lyophilized protonated protein (0.1 mM) in ^2H_2O containing 0.1 M deuterated acetic acid at pH* 4.6 and then following $^1H/^2H$ exchange using a series of $^{15}N-^1H$ PFG-HSQC spectra. The spectra were acquired with 128 × 2048 complex data points and four scans per increment, using a total experiment time of 33 min per 2D spectrum. Measurements were made over a period of 4 months, storing both NMR samples in a water bath maintained at 20 ± 1 °C between measurements. Spectra recorded on different days were normalized using the intensities of aliphatic protons measured in a 1D NMR spectrum. The peak intensities for each amide $^{15}N-^1H$ resonance were fitted to a single exponential decay using Kaleidograph (Abelbeck Software). The pH* values of these samples (4.6 ± 0.2) were verified after the $^1H/^2H$ exchange study was complete. ^1H, ^{13}C, and ^{15}N chemical shifts are referenced to the internal standard 2,2-dimethyl-2-silapentane-5-sulfonic acid (DSS), using the protocol recommended by the IUPAC−IUBMB−IUPAB Interunion Task Group on NMR Data Bases (Wishart *et al.*, 1995).

$^3J(H^N-H^\alpha)$ coupling constants were measured using a version of the PFG-HMQC-J experiment (Kuboniwa *et al.*, 1994) modified to use heteronuclear coherence selection with pulsed-field gradients for efficient solvent suppression or by 2D PFG-HNHA-J (Kuboniwa *et al.*, 1994). The spectra were acquired using 64 complex points and a spectral width of 2500 Hz in the t_1 (^{15}N) dimension and 2048 complex points and spectral width of 4550 Hz in the t_2 (H^N) dimension. A series of HMQC-J spectra were recorded with dephasing periods of 45, 50, 56, 62.5, 71.4, 83.3, and 91.0 ms and, respectively, 128 or 176 scans per increment for wt or mutant RNase A. In a similar fashion, a series of HNHA-J spectra were obtained with dephasing periods of 45, 60, 80, 100, 120, and 140 ms. Values of $^3J(H^N-H^\alpha)$ coupling constants were obtained by fitting the time dependence of the $^{15}N-H^N$ cross peak intensities as described by Kuboniwa *et al.* (1994). Coupling constants measured by HMQC-J and HNHA-J for the same amino acid residues agreed to within 0.5 Hz.

Automated Analysis of Resonance Assignments. Multidimensional NMR processing was done with Varian VNMR software and peak-picking using NMRCompass software (Molecular Simulations Inc.). Automated analysis of resonance assignments for wt and [C65S, C72S] RNase A was carried out on a Sun Sparc 10 workstation using the program AUTOASSIGN, as described by Zimmerman *et al.* (1997). Briefly, AUTOASSIGN proceeds by first identifying the backbone amide ^{15}N and $^1H^N$ resonances from each cross peak observed in 2D $^{15}N-^1H$ HSQC and 3D HNCO data and then establishing these resonances as tentative *roots* of generic (nonspecific amino acid type) spin systems (GSs). Cross peaks in the remaining 3D triple-resonance spectra whose amide ^{15}N and $^1H^N$ resonance frequencies coincide with these GS roots are then used to identify $^{13}C^\alpha$, $^{13}C^\beta$, $^1H^\alpha$, and $^{13}C'$ resonances of residue i and of the preceding residue, $i - 1$, in the sequence. In this study, these additional data were obtained from 3D HNCA, CA(CO)NH, HA(CA)NH, HA(CA)(CO)NH, CBCANH, CBCA(CO)NH, and HN(CA)CO spectra. Once the $^{13}C^\alpha$ and $^{13}C^\beta$ chemical shifts have been identified for each GS root, this information is used to derive probabilistic amino acid type scores (Zimmerman *et al.*, 1997) for both the spin system itself (i) and its predecessor ($i - 1$) in the sequence. Thus, each GS root is defined by amide $^{15}N_i$ and $^1H^N_i$ chemical shift values and

has an associated "CO ladder" specifying the resonance chemical shifts of the *preceding* amino acid residue (C^{α}_{i-1}, C^{β}_{i-1}, H^{α}_{i-1}, and C'_{i-1}), a "CA-ladder" specifying the corresponding *intraresidue* chemical shifts (C^{α}_{i}, C^{β}_{i}, H^{α}_{i}, and C'_{i}), and lists of the most probable residue types for each of its ladders. Sequence-specific assignments are then obtained by establishing the best sequential matches of chemical shifts between CO and CA ladders whose probabilistic types are consistent with the amino acid sequence. A segment of four to five sequentially linked GS spin systems is in most cases sufficient to define a unique stretch of residues in the amino acid sequence. The software iteratively establishes sequential matches and assignments of GSs to sites in the amino acid sequence until no additional information can be reliably extracted. The problem-solving methods used by AUTOASSIGN are analogous to processes used in solving a jigsaw puzzle; the sequential matching of ladders corresponds to fitting complementary-shaped pieces together, while the global constraints imposed by the image that one is trying to recreate correspond to the constraints imposed by the amino acid sequence.

RESULTS

Analytical Protein Chemistry. All NMR samples were analyzed by matrix-assisted laser desorption ion time of flight (MALDI-TOF) mass spectroscopy, N-terminal analysis, cation-exchange HPLC, and capillary electrophoresis to determine the extent of degradation, aggregation, and deamidation of the protein samples used in the NMR measurements. A representative MALDI-TOF mass spectrum and capillary electrophoresis chromatogram of wt RNase A *before* the triple-resonance data collection are shown in panels A and B of Figure 1, respectively. A capillary electrophoresis chromatogram of the sample *after* the NMR data collection is shown in Figure 1C. Mass spectroscopy, N-terminal analysis, and cation-exchange chromatography analyses (data not shown) also demonstrate that there is <2% chemical heterogeneity in these protein samples, even after more than several weeks of NMR measurements at 20 °C. Overall, these analytical protein chemisty data demonstrate that the samples were >99% homogeneous before the initiation of NMR data collection and >98% homogeneous at the end of several weeks of data collection.

Thermodynamic Properties and Enzymatic Activities of [C65S, C72S] RNase A. The activities and thermodynamic properties of wt, [C65S, C72S], and des-[65−72] RNase A are shown in Table 1. These data show that the C65−C72 disulfide bond contributes significantly to the stability of RNase A. Deletion of this disulfide bond affects both the enthalpy and entropy of folding. The large changes in enthalpy of unfolding (Table 1) suggest that alterations in the structure of folded RNase A accompany the disulfide deletion. The fact that the change in the entropy of unfolding is *smaller* in the disulfide mutant than in wt RNase A is somewhat counterintuitive, as the disulfide deletion should result in greater flexibility for the *unfolded state* and thus a larger change in entropy upon unfolding than that of the wt protein. Apparantly the disulfide deletion results in even larger changes in the entropy (e.g., flexibility) of the *folded state*. Interestingly, while the [C65S, C72S] RNase A mutant exhibits ∼23% native enzymatic activity, the previously studied des-[65−72] RNase A, in which Cys65 and Cys72

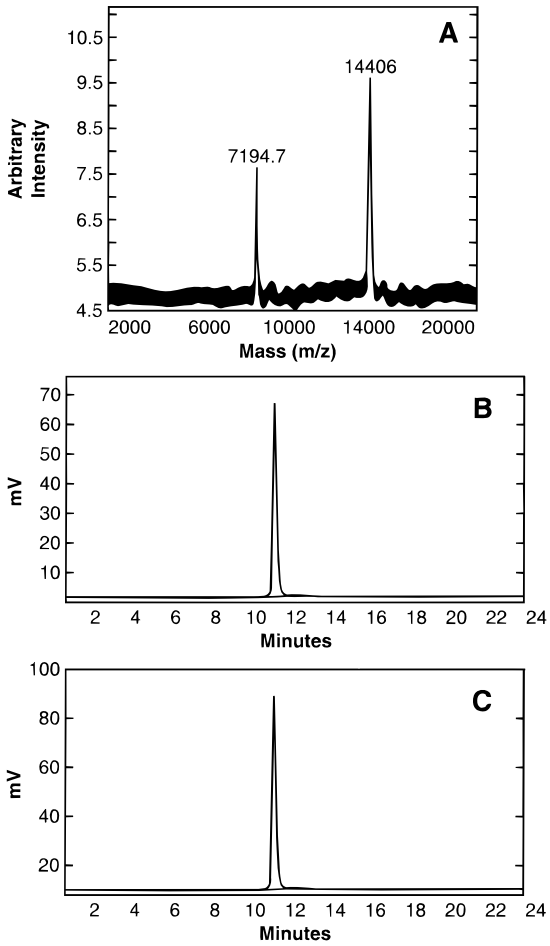

FIGURE 1: MALDI-TOF mass spectroscopy (A) and capillary electrophoresis (B, C) analyses of ^{13}C,^{15}N-enriched wt RNase A *before* (A and B) and *after* (C) triple-resonance NMR data collection. Theoretical values for 100% ^{13}C,^{15}N-enrichment are 14422.8 and 7211.4 for the $m + 1$ and $m + 2$ forms of wt RNase A. These two ion forms indicate enrichment levels of 97.7% and 95.5%, respectively, which are identical within the uncertainty in mass measurements (±0.1%) of macromolecules by MALDI-TOF mass spectroscopy.

Table 1: Thermodynamic Parameters for Unfolding and Relative Enzymatic Activities of Wild-Type and [C65S, C72S] RNase A at pH 4.6 ± 0.05

	T_m (°C)[a]	$\Delta H°$ (T_m)[a] (kcal/mol)	$\Delta S°$ (T_m)[a] (eu)	enzymatic activity[b]
wt RNase A	55.5 ± 0.2	112 ± 5	340 ± 16	100
[C65S, C72S] RNase A	38.5 ± 0.2	83.7 ± 2	269 ± 8	23 ± 2
des-[65−72] RNase A[c]	38.4 ± 0.4	80.3 ± 8	258 ± 24	81 ± 6

[a] Thermodynamic parameters are reported for the process folded to unfolded at $T = T_m$. Error estimates represent two standard deviations of multiple measurements. [b] Enzymatic activity at 22 °C relative to wt RNase A at pH 5.0, measured using cCMP substrate as described by Laity *et al.* (1993). [c] Data from Talluri *et al.* (1994).

were chemically blocked by AEMTS, has ∼80% enzymatic activity with respect to native RNase A (Talluri *et al.*, 1994).

Backbone and $^{13}C^{\beta}$ Side-Chain Resonance Assignments of wt and [C65S, C72S] RNase A. Extensive ^{1}H, ^{13}C, ^{15}N resonance assignments for both wt and [C65S, C72S] RNase A were obtained by automated analysis of triple-resonance data using the computer program AUTOASSIGN (Zimmerman & Montelione, 1995; Zimmerman *et al.*, 1997). AUTOASSIGN obtained nearly complete backbone $^{1}H^{N}$, ^{15}N, $^{1}H^{\alpha}$, $^{13}C^{\alpha}$, and $^{13}C'$ and side-chain $^{13}C^{\beta}$ assignments for both wt

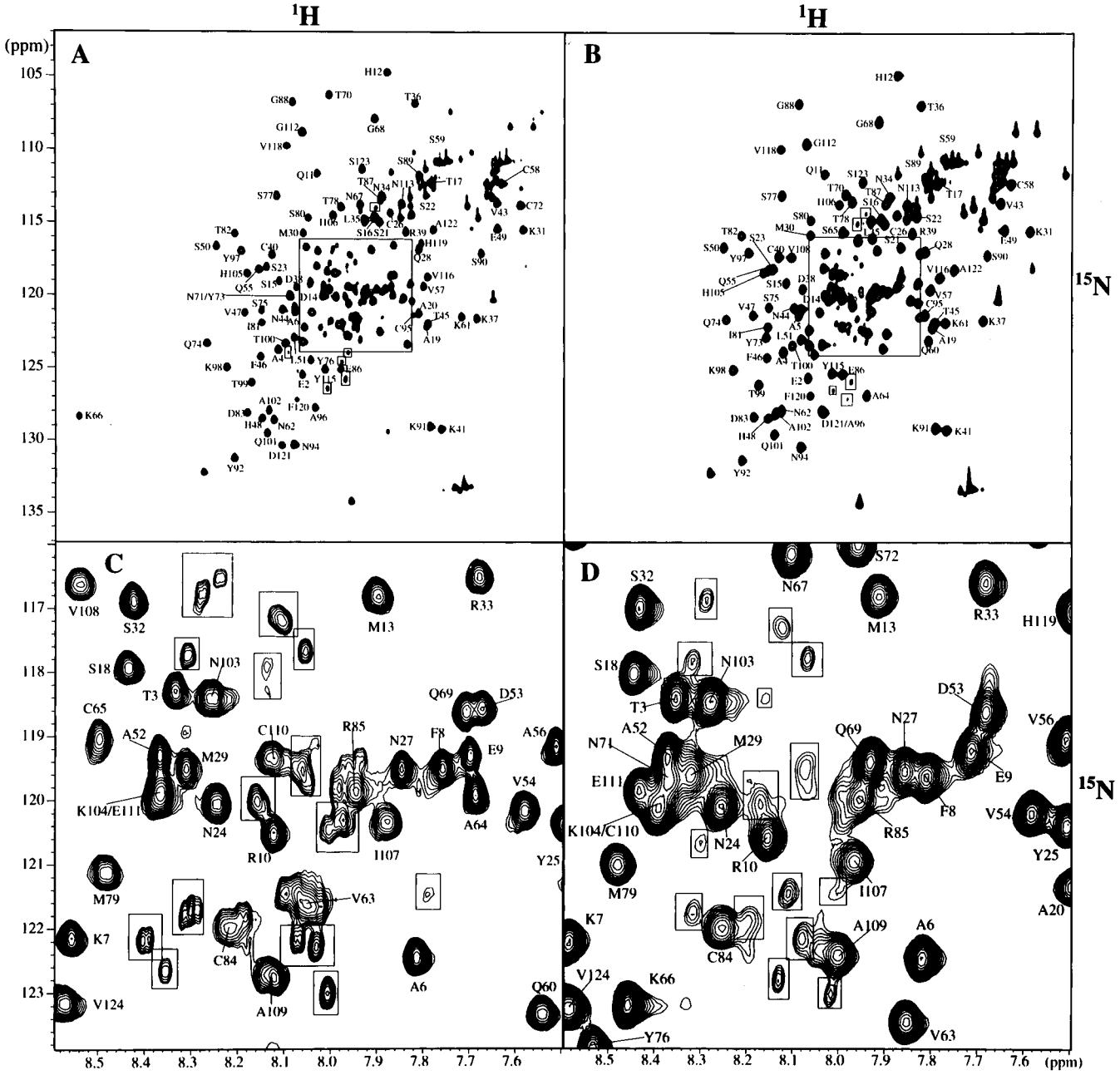

FIGURE 2: Pulsed-field gradient ^{15}N−^{1}H HSQC spectra of 2.0 mM wt (A) and 2.7 mM [C65S, C72S] (B) RNase A at pH 4.6 and 20 °C. All cross peaks are labeled with their assignments. The boxed regions in (A) and (B) are expanded in (C) and (D), respectively. Minor peaks that are visible in these spectra and in other triple-resonance spectra are boxed individually.

and mutant RNase A from these triple-resonance data. These assignments are tabulated in supplementary Tables S1 and S2, and the corresponding backbone amide proton and nitrogen assignments are indicated on plots of HSQC spectra of these proteins shown in Figure 2. Table 2 summarizes some of the more salient characteristics of the automated analysis, and a survey of the intraresidue and sequential triple-resonance connectivities determined by AUTOASSIGN for both wt and mutant RNase A is presented in Figure 3. Execution times for automated analysis of these assignments were less than 4 min using a Sun Sparc 10 workstation and a compiled version of the LISP code. Both proteins consist of 124 amino acid residues, but because the N-terminal lysine and four proline residues have no backbone amide protons, only 119 of these residues have detectable ^{15}N−^{1}H GS roots. The analyses of the wt and [C65S, C72S] RNase A data were carried out completely independently; the assignments determined for wt RNase A were *not* used in the analysis of the spectral data of the mutant. The automated analyses summarized in Table 2 and Figure 3 were subsequently verified by manual inspection of strip plots from all of the 3D triple resonance spectra. The subsequent manual analysis also provided a few additional assignments (Table 2).

In addition to resonances assigned to the predominant form of RNase A present in solution, a large number of generally weaker resonances present in these spectra (see, for example, Figure 2C,D) could be clustered into spin systems. Many of these spin systems have distinct amide ^{15}N−^{1}H roots, but their CO and CA ladders closely resemble those of assigned spin systems whose relative peak intensities are significantly stronger. Typically, the resonances of these extra spin systems have ∼10% the intensities of resonances assigned to the predominant form of the protein.

Table 2: Summary of AUTOASSIGN Analysis of Resonance Assignments for Wild-Type and [C65S, C72S] RNase A

	wt RNase A	[C65S, C72S] RNase A
no. of residues	124	124
no. of GSs[a] expected	119	119
no. of GSs obsd	149	154
no. of degenerate GS roots[b]	47	43
no. of assigned GSs	119	118
no. of extra GS spin systems	30	36
execution time (s)	233	40

no. of sequence-specific backbone and $^{13}C^{\beta}$ side-chain resonance assignments[c]	wt RNase A		[C65S, C72S] RNase A	
	automated analysis	subsequent manual analysis	automated analysis	subsequent manual analysis
$^{1}H^{N}$ (119)	119	119	118	119
^{15}N (119)	119	119	118	119
$^{1}H^{\alpha}$ (127)	125	125	125	125
$^{13}C^{\alpha}$ (124)	122	124	122	123
$^{13}C'$ (124)	122	124	122	123
$^{13}C^{\beta}$ (121)	120	120	111	117

[a] Generic spin systems (GSs) are defined in AUTOASSIGN as amino acid spin systems which have backbone amide $^{1}H^{N}$ and ^{15}N resonances. [b] Two or more GS spin systems with indistinguishable $^{1}H^{N}$ and ^{15}N chemical shifts are considered to have degenerate roots with respect to one another. [c] Numbers of possible resonance assignments based on the amino acid sequence are given in parentheses. It should be noted that the three Gly residues each have two H^{α} and no C^{β} resonances, while the four Pro residues and the N-terminal Lys residue have no backbone amide protons and do not yield detectable $^{15}N-^{1}H^{N}$ correlations.

Chemical Shift Differences between wt and [C65S, C72S] RNase A. The differences in assigned $^{1}H^{N}$, ^{15}N, $^{13}C^{\alpha}$, $^{1}H^{\alpha}$, and $^{13}C'$ backbone and $^{13}C^{\beta}$ side-chain resonance frequencies between wt and [C65S, C72S] RNase A are plotted in Figure 4. Comparison of $^{15}N-^{1}H$ HSQC spectra (Figure 2) shows that about 30% of the [C65S, C72S] RNase A cross peaks are shifted compared to those of wt RNase A. As can be seen in Figure 4, these differences are concentrated around three regions: polypeptide segments Gln60−Ser80 (β-strands[3] β2 and β3), His105−Glu111 (β-strand β6), and Ile116−Ser123 (β-strand β7). Residues containing resonances that exhibit significant chemical shift differences between wt and mutant proteins are shown on the three-dimensional X-ray crystal structure of RNase A (Wlodawer *et al.*, 1988) in Figure 5. All of the residues exhibiting significant chemical shift differences are spatially adjacent to one another in the three-dimensional structure of the mutant.

Chemical shifts are highly sensitive to local chemical and electronic environments. Since the polypeptide segment (Gln60−Ser80) includes both mutation sites, it is not surprising that the most striking chemical shift deviations occur in this region. In wt RNase A, this polypeptide segment consists of a small surface loop closed by the Cys65−Cys72 disulfide bond along with a short antiparallel β-sheet (strands β2 and β3) (Wlodawer *et al.*, 1988; Santoro *et al.*, 1993). One of these β-strands (polypeptide segment Cys72−Ser75 of strand β3) also forms antiparallel β-sheet interactions with polypeptide segment His105−Ala109 (strand β6) which, in turn, forms antiparallel β-sheet interactions with polypeptide segment His119−Val124 (strand β7). Accordingly, these chemical shift data indicate that removal of the Cys65−Cys72 disulfide bond results in structural and/or dynamical perturbations in the hydrogen-bonded β-strand network involving polypeptide segments Gln60−Ala64, Cys72−Ser80, His105−Glu111, and Ile116−Ser123, which are all located in β-sheet[3] 2 of the RNase A structure (Figure 5). Moreover, considering that chemical shifts are extremely sensitive to small structural changes, the data indicate little or no change in the protein structure distant from the local vicinity of the deleted disulfide bond. Thus, these results demonstrate that the des[65−72] three-disulfide intermediate of RNase A has an essentially native tertiary structure with perturbations localized in parts of the structure that are mostly *nearby in space* to the deleted disulfide site.

Measurements of $^{3}J(H^{N}-H^{\alpha})$ Coupling Constants. $^{3}J(H^{N}-H^{\alpha})$ coupling constants for wt and [C65S, C72S] RNase A were determined using 2D HMQC-J and HNHA-J data. These results are summarized in supplementary Table S3. Altogether, 75 and 32 reliable $^{3}J(H^{N}-H^{\alpha})$ coupling constants were determined for wt and mutant RNase A, respectively. From analyses of the curve fits for these HMQC-J and HNHA-J data, the precision of these measurements was typically better than ±5% for residues with $^{3}J(H^{N}-H^{\alpha})$ values greater than ∼5 Hz. However, comparison of values measured for wt RNase A with values back calculated from the 1.26 Å X-ray crystal structure (Wlodawer *et al.*, 1988) using the Karplus curve described by Pardi *et al.* (1984) demonstrates that, for values greater than ∼5 Hz, the differences between back-calculated and observed coupling constants can be as large as ±1.5 Hz; for smaller $^{3}J(H^{N}-H^{\alpha})$ values the differences between measured and back-calculated values were somewhat larger. These differences, representing the apparant accuracy of these measurements, reflect several factors including systematic errors in the methods of measurements, differences between solution and crystal structures, and dynamical averaging which occurs in the solution structure. From these considerations the differences between $^{3}J(H^{N}-H^{\alpha})$ coupling constants measured for wt and mutant RNase A were conservatively interpreted to be significant only if they were greater than 1.5 Hz. Most $^{3}J(H^{N}-H^{\alpha})$ values were quite similar (within ±1.0 Hz) in wt and mutant RNase A. Significant differences, however, were observed for residues Gln60 ($\Delta J \geq 3.7$ Hz), Cys72 ($\Delta J \approx 1.5$ Hz), Thr82 ($\Delta J \geq 2.8$ Hz), and Val124 ($\Delta J \geq 2.2$ Hz) (supplementary Table S3).

Backbone Amide $^{1}H/^{2}H$ Exchange Rates. The exchange rates of amide protons at pH* 4.6 and 20 °C were measured using a series of $^{15}N-^{1}H$ HSQC spectra. There were 85 and 70, respectively, slowly exchanging amide protons (defined as those with exchange rate constants ≤ 0.1 min^{-1}) in wt and [C65S, C72S] RNase A. The locations of these slowly exchanging amides in the protein sequence are indicated in Figures 6 and 7. The high sensitivity of the PFG-HSQC experiments used in these measurements enabled us to characterize an additional 30 slowly exchanging amide protons than have been reported in previous studies of wt RNase A (Robertson *et al.*, 1989; Santoro *et al.*, 1993; Talluri *et al.*, 1994). The newly observed slowly exchanging amide protons are all located in well-defined elements of backbone structure, and many of them are involved in the backbone hydrogen bond network (Wlodawer *et al.*, 1988; Santoro *et*

[3] The designations of β-sheets used in this paper are based on the locations of β-strands reported in the Brookhaven Protein Data Bank (PDB) entry 9RSA: β1, sheet 1, strand 1; β2, sheet 2, strand 1; β3, sheet 2, strand 2; β4, sheet 1, strand 2; β5, sheet 1, strand 3; β6, sheet 2, strand 3; and β7, sheet 2, strand 4.

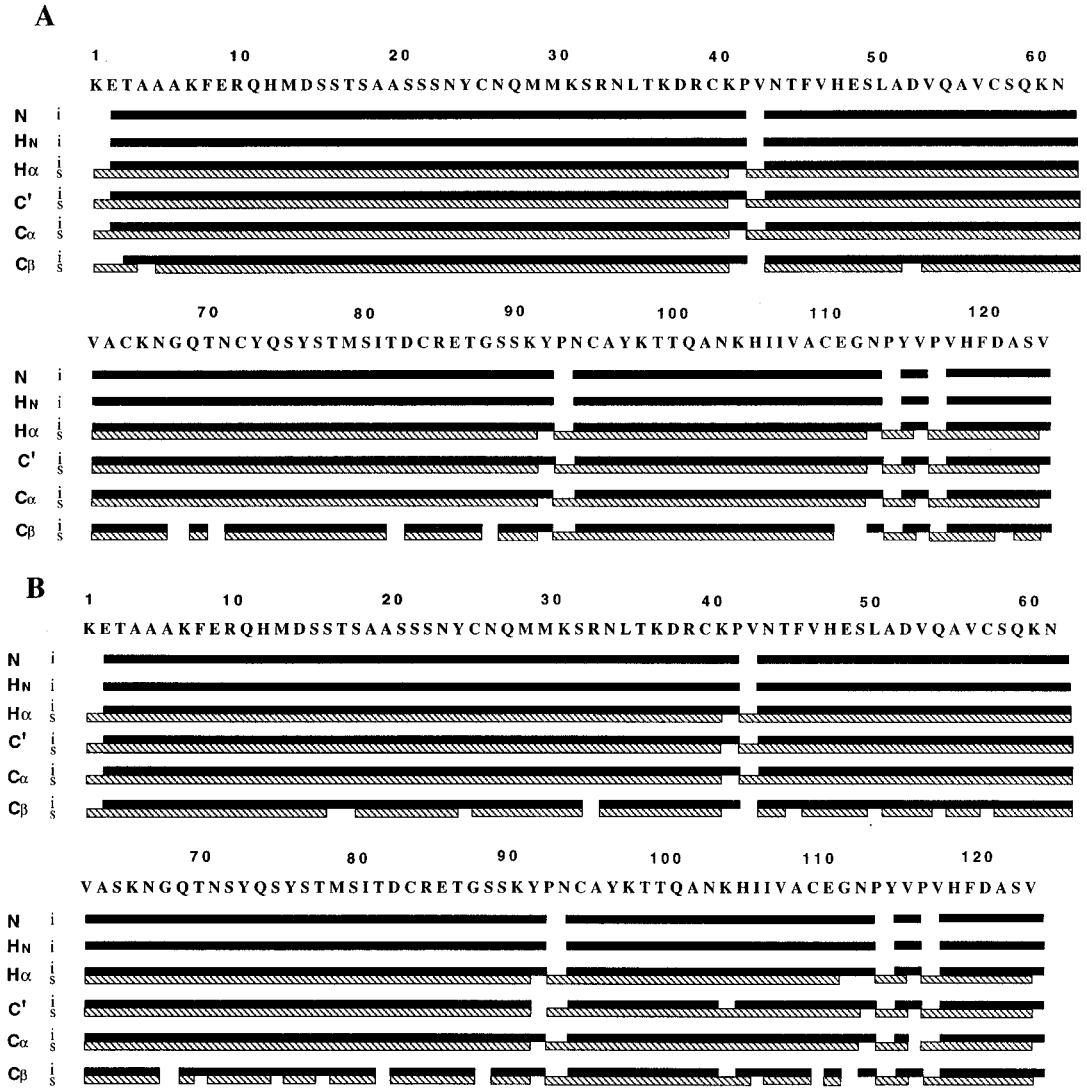

FIGURE 3: Summary of intraresidue and sequential connectivity data determined by AUTOASSIGN for wild-type (A) and [C65S, C72S] (B) RNase A at pH 4.6 and 20 °C. Solid and hatched lines indicate intraresidue (i) and sequential (s) residue connectivities, respectively.

al., 1993). All of these newly observed "slowly" exchanging amide protons in wt RNase A do, in fact, exhibit faster exchange rates than the set of slowly exchanging amide protons reported previously.

For all of the amide protons of the core β-sheet, the $^1H/^2H$ exchange rate constants are much larger in [C65S, C72S] RNase A than in wt RNase A (Figure 8). Some sites exhibit as much as 10^4-10^8 faster exchange in the mutant than in wt RNase A. A comparison of $^1H/^2H$ exchange rate constants for backbone amides of [C65S, C72S] and wt RNase A, $\log(k_{mut}/k_{wt})$, is shown in Figure 9 on the three-dimensional structure of wt RNase A. It is clear from this figure that the exchange rate constants are increased throughout the whole [C65S, C72S] RNase A molecule. Close examination of Figure 9 reveals that the amide protons with differences in the exchange rate constants $k_{mut}/k_{wt} > 10$ between wt and [C65S, C72S] RNase A are located mainly in the core β-sheet regions. These measurements indicate that the rates of amide proton exchange in the core β-sheets of RNase A are affected more by the removal of the C65−C72 disulfide bond than those in other regions such as the α-helices.

Comparisons of Hydrogen-Bonded Backbone Structures of wt and [C65S, C72S] RNase A. Summaries of $^{13}C^\alpha$ chemical shift deviations from statistical coil values (Thanabal *et al.*, 1994) for both wt and [C65S, C72S] RNase A are shown in supplementary Figure S10. These conformation-dependent chemical shifts provide a qualitative characterization of $\phi-\psi$ backbone conformations for each residue in these protein structures (Spera & Bax, 1991). Small conformation-dependent $^{13}C^\alpha$ chemical shifts ($\Delta\delta C^\alpha = \delta C^\alpha_{obs} - \delta C^\alpha_{coil}$) are nearly identical in wt and mutant RNase A for α-helices α1, α2, and α3, for β-strands β1, β4, and β5, and for the intervening loop segments. The $\Delta\delta C^\alpha$ differences between wt and [C65S, C72S] RNase A are localized in and near β-strands β2, β3, β6, and β7 of β-sheet 2. These chemical shift data further demonstrate that the backbone structures of wt and mutant RNase A are very similar, except in the local three-dimensional vicinity of the disulfide deletion site.

Surveys of short- and medium-range NOE and amide $^1H/^2H$ exchange rate data for wt and mutant RNase A are presented in Figure 6. These data clearly delineate three α-helices (α1, Thr3−Met13; α2, Asn24−Asn34; and α3, Ser50−Gln60) in both wt and [C65S, C72S] RNase A. An analysis of interstrand backbone−backbone NOEs in wt and mutant RNase A is presented in Figure 7. Hydrogen bonds were identified unambiguously on the basis of *both* inter-

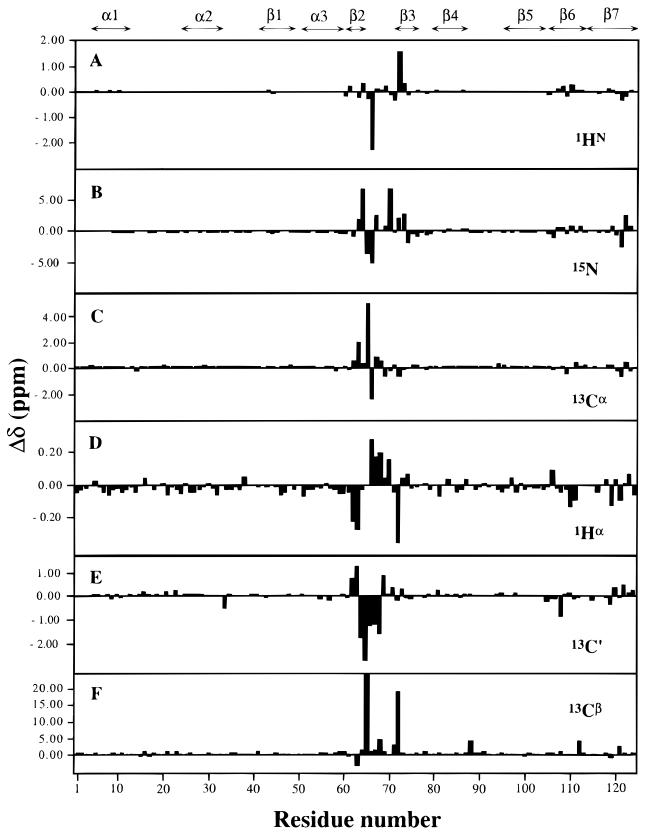

FIGURE 4: Differences in chemical shifts ($\Delta\delta = \delta_{mut} - \delta_{wt}$) between wt and [C65S, C72S] RNase A, plotted as a function of residue number for $^1H^N$ (A), ^{15}N (B), $^{13}C^\alpha$ (C), $^1H^\alpha$ (D), $^{13}C'$ (E), and $^{13}C^\beta$ (F), respectively. Regular backbone structures indicated by arrows are based on the X-ray crystal structure[3] (Wlodawer *et al.*, 1988).

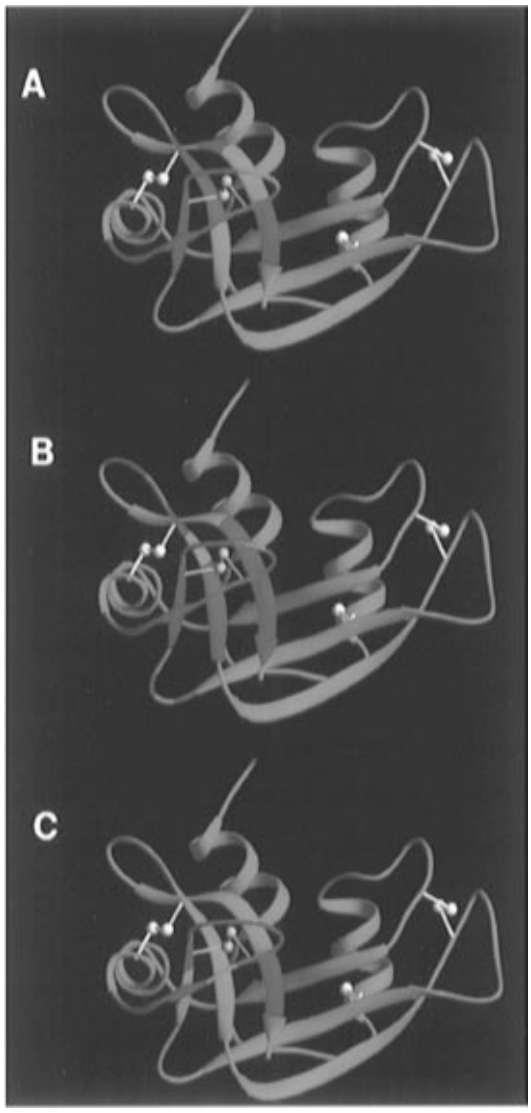

FIGURE 5: Ribbon drawing based on the crystallographic atomic coordinates (Wlodawer *et al*., 1988) of wt RNase A obtained from the Brookhaven Protein Data Bank (PDB entry 9RSA). The four native disulfide bonds are shown in white (disulfides C40−C95, C58−C110, and C26−C84) and yellow (disulfide C65−C72). The residues exhibiting significant differences in the chemical shifts ($\Delta\delta$) between wt and [C65S, C72S] RNase A are highlighted on the structure in red for (A) $^1H^N$ ($|\Delta\delta| > 0.1$ ppm), (B) ^{15}N ($|\Delta\delta| > 0.5$ ppm), and (C) $^{13}C^\alpha$ ($|\Delta\delta| > 0.5$ ppm).

strand NOEs and slowly exchanging amide protons. It is evident from Figures 6 and 7 that the overall α-helical and β-sheet structure of wt RNase A is preserved in [C65S, C72S] RNase A. These results further demonstrate that the regularly ordered backbone structures of [C65S, C72S] RNase A and wt RNase A are quite similar.

Subtle Structural Differences between wt and [C65S, C72S] RNase A. In order to account for the large differences in thermal stability for wt and [C65S, C72S] RNase A, small differences in NOE intensities and $^3J(H^N-H^\alpha)$ coupling constant data have been examined in more detail. One clear structural change arising from the removal of the C65−C72 disulfide bond is the disruption of the short antiparallel β-sheet [between β-strands corresponding to polypeptide segments 60−64 (β2) and 72−75 (β3)] and of the loop structure between these β-strands. The hydrogen bond network connecting these two β-strands in wt RNase A involves the amide protons of residues Lys61, Val63, Cys72, and Gln74. All of these were identified as slowly exchanging amide protons from amide $^1H/^2H$ exchange measurements for wt RNase A (Figure 6). The expected interstrand NOEs involving $61H^N-74H^N$, $61H^N-75H^\alpha$, $62H^\alpha-74H^N$, $63H^N-72H^N$, $63H^N-73H^\alpha$, and $64H^\alpha-72H^N$ were also observed for wt RNase A. In addition, the slowly exchanging amide proton of Tyr73 is attributed to an interstrand hydrogen bond formed with the backbone carbonyl oxygen of Val108 (Figure 7). In contrast, for [C65S, C72S] RNase A, the only slowly exchanging amide protons observed in this region are those of Val63, Ser72, Tyr73, and Gln74; the hydrogen bond involving the amide proton of Lys61 and backbone carbonyl of Gln74 is disrupted in this mutant. Difference in dihedral angle ϕ of residue Gln60 is also indicated by the $^3J(H^N-H^\alpha)$ coupling constant measurements, as described above. In addition to the changes in the hydrogen bond network of β-sheets, the turn structure of wt RNase A involving polypeptide segment Ala64−Gln69 exhibits structural perturbations. In contrast to wt RNase A, residues Ala64, Cys65, Gly68, and Gln69 in this loop structure do not exhibit slowly exchanging amide protons in [C65S, C72S] RNase A (Figures 6 and 7). Moreover, the interstrand $65H^N-69H^N$ NOE and the hydrogen bond indicated by slow exchange of the amide proton of Cys65 in wt RNase A are not present in [C65S, C72S] RNase A. Other amide protons that are slowly exchanging in wt RNase A but not in the mutant include those of residues Val43, Asn44, and Thr45 (Figures 6 and 7). Subtle structural disruption is also indicated in this region of the protein by the interstrand H^N-H^N NOE that is observed for Asn44 in wt RNase but not in

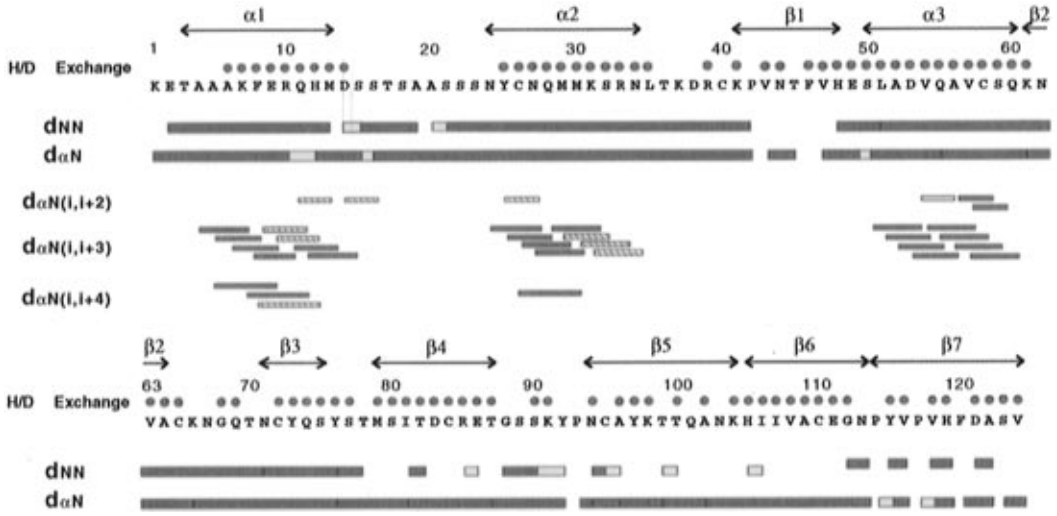

FIGURE 6: Survey of slowly exchanging amide protons (circles) and characteristic short-range NOEs involving H^N protons (rectangles) identified from NMR data for wt and [C65S, C72S] RNase A at pH* 4.6 and a temperature of 20 °C. Blue circles indicate that the corresponding amide proton was characterized as slowly-exchanging in both the wt and mutant samples, while red circles indicate that the corresponding amide proton is slowly exchanging in wt RNase but not in the mutant protein. NOEs indicated in blue were observed in both wt and mutant proteins, those in red were observed only in wt RNase, and those in yellow were observed only for [C65S, C72S] RNase A. The NOEs indicated in hatched blue were clearly observed in wt or mutant and were overlapped with other peaks in the mutant or wt spectra, respectively.

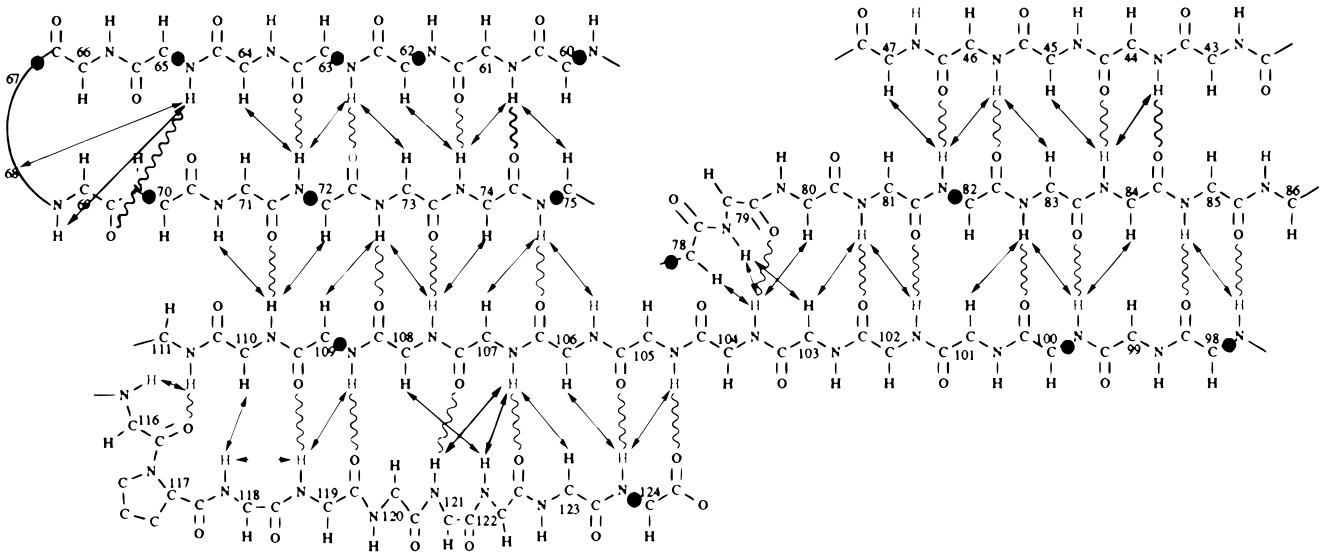

FIGURE 7: Schematic diagram showing β-strands identified for wt and [C65S, C72S] RNase A by NMR analysis at pH* 4.6 and a temperature of 20 °C. Double-headed arrows denote short distances manifesting NOEs assigned in the 2D homonuclear and/or 3D ^{15}N-edited NOESY-HSQC spectra. These β-sheet structures were corroborated by identification of slowly exchanging amide protons associated with hydrogen bonds, indicated by rippled lines. NOEs and hydrogen bonds indicated in blue were identified in *both* wt and mutant proteins, while NOEs and hydrogen bonds indicated in red were observed only in wt RNase. Blue circles indicate residues for which backbone $^3J(H^N-H^\alpha)$ coupling constants are similar for wt and mutant ($|\Delta J| < 1.5$ Hz) or that the data provided only upper-bound values of $^3J(H^N-H^\alpha)$ which could not be used to identify structural change, and red circles indicate residues for which backbone $^3J(H^N-H^\alpha)$ coupling constants are significantly different ($|\Delta J| \geq 1.5$ Hz).

[C65S, C72S] RNase A (Figure 7). Similar observations indicating subtle structural alterations were also observed in the vicinity of the Ala122 H^N amide proton (Figures 6 and 7). Accordingly, on the basis of combined analysis of $^1H/^2H$ exchange with NOE and/or $^3J(H^N-H^\alpha)$ coupling constant data, we conclude that hydrogen bonds involving amide protons of residues Asn44, Lys61, Cys65, Gly68, Gln69, and Ala122 are altered in [C65S, C72S] RNase A. The disruption of these hydrogen bonds contributes to the lower enthalpic stability of this disulfide mutant. Other small differences in NOE intensities, $^3J(H^N-H^\alpha)$ coupling constants, and amide $^1H/^2H$ exchange rates (e.g., at sites Val43, Thr45, Ala64, Thr82, and Val124) probably also reflect subtle structural changes which cannot be characterized accurately from the available data.

DISCUSSION

Both wt RNase A and an analog of a folding/unfolding intermediate, [C65S, C72S] RNase A, were analyzed using heteronuclear NMR techniques. The high sensitivity and resolution of these methods provide a more detailed and accurate characterization of solution structures of these proteins than has previously been possible. These data provide new insights into the role of the C65−C72 disulfide bond in the folding and unfolding mechanisms.

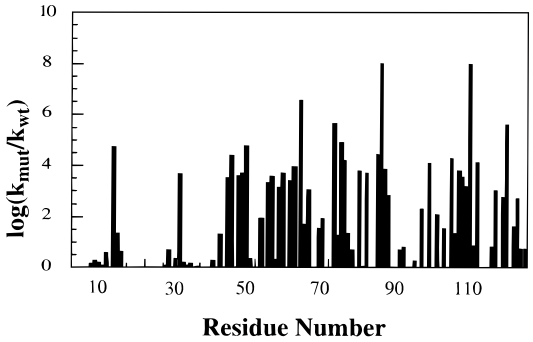

FIGURE 8: Ratios of amide $^1H/^2H$ exchange rate constants, k_{mut} and $k_{wt,}$ for [C65S, C72S] and wt RNase A, plotted as a function of residue number.

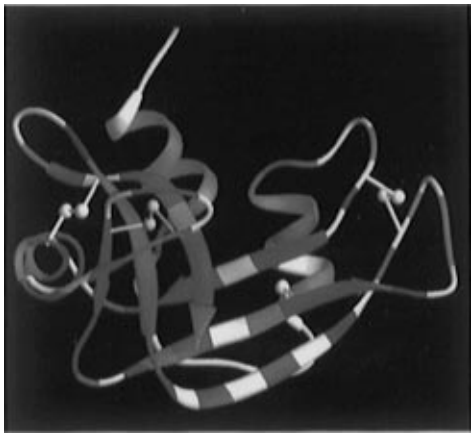

FIGURE 9: Ratios of relative amide $^1H/^2H$ exchange rate constants, k, for [C65S, C72S] and wt RNase A, highlighted on the three-dimensional structure of wt RNase A. Residues shown in red exhibit $\log(k_{mut}/k_{wt}) > 1.0$, those in blue exhibit values $1.0 \geq \log(k_{mut}/k_{wt}) > 0.1$, and those in white $k_{mut} \approx k_{wt}$. Residues shown in gray are those for which amide proton exchange rates could not be measured reliably in one or both of the protein samples.

Automated Analysis of Resonance Assignments. The use of automated assignment software, together with a robust strategy for triple-resonance data collection, greatly reduced the time required for determining resonance assignments of backbone ($^1H^N$, ^{15}N, $^1H^\alpha$, $^{13}C^\alpha$, and $^{13}C'$) and side-chain $^{13}C^\beta$ nuclei. The entire assignment process, including data collection, processing, peak-picking, and analysis, was completed in 2 weeks for each protein. Of these 2 weeks, 10 days were devoted to data collection. Execution times for running AUTOASSIGN were under 4 min for each protein. The automated analysis was subsequently verified by manual analysis of these same 3D triple resonance spectra and by analysis of sequential (Figure 6) and long-range (Figure 7) NOEs consistent with these assignments and the known three-dimesional structure of RNase A. These assignments are also in generally good agreement with published H^N and H^α proton assignments for wt RNase A (Rico *et al.*, 1989; Robertson *et al.*, 1989; Santoro *et al.*, 1993).

Although the sequence-specific assignments for wt and [C65S, C72S] RNase A were derived independently of one another, the NMR experiments carried out for this study could also provide a data base for development of "homology-based" automated assignment software. In such a strategy, assignments obtained from a complete set of triple-resonance spectra for wt RNase A could be used to guide the interpretation of a more limited set of spectra for [C65S, C72S] RNase A. More generally, if a second protein contains high sequence homology to a protein whose assignments and structure have been determined previously, these known assignments can be used to assign the homologous regions first, thus restricting the possible assignments of the remaining nonhomologous regions and dramatically reducing the data collection and software execution time. In the automated analysis reported here, homology-based reasoning was not used, and the spectra of both proteins were analyzed independently (and without knowledge of the published proton assignments). The fact that all chemical shift differences are located nearby in three-dimensional space to the site of the disulfide deletion provides a strong validation of the robustness of the AUTOASSIGN analysis. Work is now in progress to determine how homologous assignment information can be used to reduce the number of triple-resonance data sets required to provide reliable and complete resonance assignments.

Chemical Shifts and Regular Backbone Structure of wt and [C65S, C72S] RNase A. It is a well-established fact that chemical shifts are very sensitive to subtle changes in nuclear environments. Therefore, a comparison of the chemical shifts for wt and [C65S, C72S] RNase A should be a good indicator of even small structural changes. Figure 5 illustrates the distribution of differences in chemical shifts for these two proteins, highlighted on the crystal structure of wt RNase A. It is clear from this figure that the most significant differences are located in regions of the structure that are nearby in three-dimensional space to the mutation sites. The removal of the disulfide bond C65−C72 directly affects chemical shifts of three spatially adjacent regions (Gln60−Ser80 including β-strands β2 and β3, His105−Glu111 including β-strand β6, and Ile116−Ser123 including β-strand β7). This is particularly significant, as these antiparallel β-sheets of wt RNase A are considered to form a major portion of the hydrophobic core of RNase A which comprises polypeptide segment Pro42−His48, Asn71−Thr86, Ala96−Glu111, and Val116−Val124 (Matheson & Scheraga, 1978). These effects of Cys65−Cys72 disulfide deletion on the core β-sheet structure are not surprising since polypeptide segment Gln60−Ser80 forms antiparallel β-sheet interactions with segment His105−Glu111.

The similarities of chemical shifts between wt and [C65S, C72S] RNase A in the rest of the structure are striking. The standard deviations of the differences in the chemical shifts for the residues of polypeptide segments 1−60 and 81−104 are 0.02, 0.11, 0.08, 0.04, and 0.06 ppm for $^1H^N$, ^{15}N, $^{13}C^\alpha$, $^{13}C'$ and $^1H^\alpha$ nuclei, respectively. These values are more or less within the digital resolutions of the data collected for these nuclei, with the exception of $^1H^\alpha$. In fact, the standard deviation for $^1H^\alpha$ chemical shift differences was three times the value of the digital resolution. The larger dispersion in the differences in $^1H^\alpha$ chemical shifts throughout wt and [C65S, C72S] RNase A can be attributed to the fact that ^1H chemical shifts are more sensitive to slight changes in both structure and environment than those of other nuclei, and other subtle structural changes appear to occur in regions of the protein that are distant from the mutation site.

Specific information about regularly ordered backbone structure can also be inferred from analysis of the $^{13}C^\alpha$ chemical shift deviations from expected statistical coil values because these deviations are directly correlated with backbone conformation (Spera & Bax, 1991). The backbone

structure information inferred from analysis of the $^{13}C^{\alpha}$ chemical shift data was further confirmed by NOE, $^{3}J(H^{N}-H^{\alpha})$ coupling, and amide proton $^{1}H/^{2}H$ exchange data. On the basis of similarities in chemical shifts among the two proteins, comparisons of slowly exchanging amide protons, and NOE data, we conclude that the overall backbone structures for wt and [C65S, C72S] RNase A are quite similar. Moreover, the partial native activity of [C65S, C72S] RNase A confirms the presence of the correct active site conformation in this mutant.

Changes in Internal Hydrogen Bonding. Although their overall structures are very similar, the NMR data for the core β-sheets (Figure 7) indicate that some hydrogen bonds of the wt RNase A structure are disrupted in [C65S, C72S] RNase A. Specifically, the combined NOE and amide proton exchange rate data indicate that the wt interstrand hydrogen-bonded amides of residues Asn44, Lys61, Cys65, Gly68, Gln69, and Ala122 are altered in this mutant. Significantly, while large chemical shift differences between wt and mutant proteins are observed for all residues in polypeptide segments Gln60−Ser80, His105−Glu111, and Ile116−Ser123, which include several of these disrupted hydrogen bonds, the resonance frequencies of residue Asn44 are not greatly perturbed.

Significance of the C65−C72 Disulfide Bond for Oxidative Folding/Unfolding. The C65−C72 disulfide bond is one of the first to be broken during the reductive unfolding of wt RNase A (Rothwarf & Scheraga, 1991; Li *et al.*, 1995). Two previous studies involving des-[65−72] RNase A offer some insight as to the significance of this disulfide bond. In a kinetic study (Li *et al.*, 1995), the rate of reduction of the next disulfide bond in des-[65−72] RNase A was observed to be five times greater than the rate of reduction of the first disulfide bond (i.e., C65−C72) in wt RNase A at 25 °C. Talluri *et al.* (1994) used NMR spectroscopy to determine that this polypeptide segment is largely disordered in des-[65−72] RNase A. These structural alterations were proposed to make the other three disulfide bonds more accessible to solvent and reducing reagent. In addition, while the conformational chemical potential difference, $\Delta\Delta\mu^{\circ}_{conf}$ (Konishi *et al.*, 1982b), between wt and [C65S, C72S] RNase A was found to be 5.2 ± 0.3 kcal/mol (determined at 47 °C, the temperature midpoint between the melting temperatures of the two proteins), a theoretical loop entropy calculation (Lin *et al.*, 1984) of the enhanced stability of the unfolded protein due to loss of the C65−C72 disulfide cross-link accounted for only 3.9 kcal/mol. The remaining 1.3 kcal/mol of free energy stabilization was therefore attributed (Talluri *et al.*, 1994) to additional enthalpic and entropic contributions arising from changes in the structure of the Cys65−Cys72 region, since this was the only part of the structure found to be different between wt and des-[65−72] RNase A.

Our results indicate that the removal of the C65−C72 disulfide bond has more widespread effects on the structure and dynamics of the protein than was previously suspected. In particular, although there is relatively little change in the overall chain fold of the protein, the tertiary structure of the β-sheet core of [C65S, C72S] RNase A is altered relative to that of wt RNase A. The chemicial shift, NOE, $^{3}J(H^{N}-H^{\alpha})$ coupling, and amide exchange data reveal subtle structural perturbations throughout β-sheet 2, comprising part of the hydrophobic core of RNase A. Changes in hydrogen-bonding and packing interactions of this β-sheet core also contribute to the enthalpic effects cited by Talluri *et al.* (1994). Such enthalpic coupling between disulfide bond formation and the stability of the protein core has been suggested in other studies (Laskowski & Scheraga, 1954; Betz, 1993; Mücke & Schmid, 1994). According to the present study, these enthalpic effects include numerous subtle stabilizing interactions within wt RNase that are affected by reduction (or deletion) of the C65−C72 disulfide bond.

Our thermodynamic measurements also indicate that the difference in entropy between folded and unfolded states is *smaller* for both des-[65−72] and [C65S, C72S] RNase A than for the wt protein. This contradicts the theoretical loop entropy calculations (Talluri *et al*., 1994) which indicated that this disulfide deletion should *increase* the entropy differences between folded and unfolded states. We interpret these entropy measurements as evidence that a signficant change in conformational flexibility of the folded state accompanies the C65−C72 disulfide deletion. Thus, the differences in stabilities of wt and disulfide-deleted RNase A arise from a combination of structural changes in the polypeptide segment Cys65−Cys72, relatively small structural alterations of the hydrophobic core, and dynamical differences between the wt and mutant proteins.

The observed structural changes, localized primarily within β-sheet 2, also correlate with changes in global amide proton exchange rates. The changes in conformational flexibility indicated by the thermodynamic measurements may contribute to the enhanced rates of amide proton exchange observed for [C65S, C72S] RNase A. However, as discussed in more detail below, the observed changes in amide $^{1}H/^{2}H$ exchange rates may be due to lower thermodynamic stability of the mutant RNase A, higher conformational dynamics of the mutant protein, or a combination of both effects. Regardless of the cause, the observed higher amide proton exchange rates should correlate with higher accessiblity of reducing agent to the core disulfide bonds, making further reduction of disulfide bonds more rapid in this disulfide mutant.

Disulfide Deletions in Other Proteins. The structural and thermodynamic consequences of disulfide deletion by chemical modification or site-directed mutagenesis have been studied in other proteins, including bovine pancreatic trypsin inhibitor (BPTI) (Eigenbrot *et al*., 1990; Naderi *et al*., 1991; van Mierlo *et al*., 1991; Hurle, *et al*., 1992; Staley & Kim, 1992) and ribonuclease T1 (Mayr *et al*., 1994; Mücke & Schmid, 1994). In both of these systems, the deletion of a single disulfide bond has minimal effects on the overall structure of the protein but decreases the thermal stability significantly. Although the general effects of a single disulfide deletion are similar in BPTI, RNase T1, and RNase A, the roles of these various species with non-native pairings of disulfide bonds in oxidative folding mechanisms are quite different.

Significant Changes in Amide Proton Exchange Rates Reveal Global Destabilization of the [C65S, C72S] RNase A Structure. The exchange rates of amide protons can provide information about the equilibrium between the folded and unfolded (or partially unfolded) states of proteins and/or information about conformational dynamics (Hvidt & Nielsen, 1966). A detailed analysis of the amide $^{1}H/^{2}H$ exchange protection factors of wt and [C65S, C72S] RNase A indicates that the effect of deletion of the C65−C72

disulfide bond on these exchange rates is *not uniform* throughout the molecule (data not shown). While ratios of exchange rate constants (i.e., k_{mut}/k_{wt}) in the mutation site and in the β-sheet core regions vary from 10 to 10^8, the values of this ratio for the α-helices and other parts of the structure are mostly less than 10 (see Figures 8 and 9). Although the increase in the exchange rate may be attributed to a general increase in the population of unfolded (or partially unfolded) molecules, the removal of the C65−C72 disulfide bond appears to affect exchange rates in the β-sheet core more than in other hydrogen-bonded structures. This appears to be due to the fact that the amide proton exchange rates are faster, and protection factors smaller, in these α-helices than in the β-sheet core. A more detailed analysis of the exchange rates is necessary to interpret this phenomenon in terms of exchange mechanisms (Hvidt & Nielsen, 1966) and the free energies of global vs local unfolding (Englander *et al.*, 1972; Hilton & Woodward, 1979). However, the observed effects of the C65−C72 disulfide deletion on the exchange rates of amides located throughout the RNase A structure are consistent with the conclusion that the destabilization of the β-sheet core by this disulfide deletion leads to the global destabilization of [C65S, C72S] RNase A.

Enzymatic Activity of [C65S, C72S] RNase A. The previously studied trapped folding intermediate, des-[65−72] RNase A, in which residues Cys65 and Cys72 were chemically blocked, has 80% native enzymatic activity (Talluri *et al.*, 1994), while [C65S, C72S] RNase A is only 23% active. It should be emphasized that this difference (80% vs 23% native activity) represents a very small change in free energy and may arise from very subtle effects. The blocking reagent, AEMTS, used in the previous study (Talluri *et al.*, 1994) carries a reactive group on one end and a positively charged ammonium group on the other end (Rothwarf & Scheraga, 1991). After reaction with cysteines 65 and 72, this positively charged group could affect the active site of des-[65−72] RNase A by stabilizing substrate binding in the complex and thus serve a function similar to that of the highly conserved Lys66 (Blackburn & Moore, 1982). Residues Lys66 and Asn67 are completely conserved in all mammalian pancreatic RNase A's, and the loop region encompassing C65−C72 has been shown to play a crucial role in determining affinity and specificity of RNase A activity (Blackburn & Moore, 1982; Beintema *et al*., 1988).

Minor Conformers of wt and [C65S, C72S] RNase A. As can be seen from Figure 2, there are a number of minor peaks in the $^{15}N-^{1}H$ HSQC spectra of both wt and [C65S, C72S] RNase A. Minor resonances associated with these ^{15}N and ^{1}H resonances were also detected in many of the 3D triple-resonance spectra. These minor peaks are present from the beginning of the NMR data collection, and their positions and intensities do not change with time. Automated analysis of these triple-resonance data with AUTOASSIGN indicates that there are some 30 and 36 extra spin systems for wt and [C65S, C72S] RNase A, respectively (Table 2). Most of these spin systems include both backbone N, C, and H and side-chain C^{β} resonances. Chemical heterogeneity of these protein samples is excluded as the source of these extra spin systems considering the high purity indicated by mass spectroscopy, cation-exchange chromatography, and capillary electrophoresis analysis both before and after the NMR measurements (see, for example, the data summarized in Figure 1). An alternative explanation for these extra spin systems is *conformational* heterogeneity. In fact, the presence of multiple side-chain conformers of wt RNase A has been reported in previous X-ray crystallography and high-resolution NMR studies (Wlodawer *et al.*, 1988; Santoro *et al.*, 1993). Buckler *et al.* (1995) have interpreted fluorescence energy transfer measurements as evidence for significant flexibility in the N-terminal polypeptide segment of wt RNase A; their data indicate a subpopulation (∼10%) of molecules in which the N-terminal polypeptide segment is largely disordered. Multiple conformational ensembles of native proteins differing in cis/trans X−Pro peptide bond conformations have been reported in NMR studies of several other proteins [see, for example, Evans *et al.* (1989), Chazin *et al.* (1989), Kördel *et al.* (1990), and Moy *et al.* (1995)]. Accordingly, it is possible that the minor amino acid spin systems detected in our triple-resonance NMR spectra also arise from multiple conformations of RNase A in slow (i.e., conformational lifetimes >1 ms) dynamic equilibrium with the folded, native structure. Further efforts to characterize structural differences between these major and minor conformational states of native RNase are now in progress.

Conclusions. Kinetic studies (Li *et al.*, 1995) show that reduction of the C65−C72 disulfide bond is one of the rate-determining steps in the reductive unfolding of RNase A. Assuming that [C65S, C72S] RNase A is a valid analog of this three-disulfide intermediate, one conclusion of this NMR study is that formation of des-[65−72] RNase A from native RNase A in the reductive unfolding pathway involves structural changes in the backbone and/or side-chain conformations of some β-strands (i.e., β1, β2, β3, β6, and β7), partially disrupting the hydrogen-bonded network in the hydrophobic core of the protein. This disruption of the hydrophobic core is a direct consequence of the removal of the C65−C72 disulfide bond. These structural changes result in an enthalpic destabilization of the folded state of [C65S, C72S] RNase A relative to the wt protein. In addition, the relatively larger entropy of the unfolded three-disulfide form of RNase A (compared with the four-disulfide wt form) which acts to stabilize the unfolded state appears to be partially compensated by an even larger enhanced entropy of the folded state. This results in a smaller entropy difference $\Delta S°$ between folded and unfolded states of the mutant than between the corresponding states of the four-disulfide wt protein.

In the oxidative folding of RNase A, 80% of the molecules fold through the formation of the des-[40−95] three-disulfide intermediate, and only 20% of the molecules fold through the formation of the des-[65−72] three-disulfide intermediate (i.e., the "minor" pathway; Li *et al.*, 1995). Although the structural organizations occurring in the steps leading up to the appearance of the des-[65−72] folding intermediate on this minor oxidative folding pathway are not yet characterized, formation of the fourth disulfide bond on this pathway functions to "lock in" the native-like structure already present in this three-disulfide intermediate. This process of "locking in" native structure involves subtle structural changes throughout the β-sheet core and results in a native RNase A molecule with much slower amide proton exchange rate constants than those of des-[65−72] RNase A. Although it is evident from our thermodynamic measurements that the entropy difference $\Delta S°$ between folded and unfolded states of three-disulfide des-[65−72] and [C65S, C72S] RNase A

analogs is smaller than for the four-disulfide wt protein, it is not yet clear if the relatively rapid amide proton exchange rate constants measured for [C65S, C72S] RNase A reflect enhanced dynamics of the folded protein structure due to disulfide deletion of if they simply reflect the altered thermodynamic stability of the hydrogen-bonded core. Further NMR studies aimed at quantifying these dynamic differences between analogs of oxidative folding intermediates and native RNase A are in progress in our laboratories.

ACKNOWLEDGMENT

We thank M. E. McDonald for help in sample preparations and M. Tashiro, B. A. Lyons, B. Celda, R. Watson, and T. W. Thannhauser for their experimental assistance and valuable suggestions. We also thank R. T. Raines of the University of Wisconsin for providing the expression vector pXBR-2, R. Schiksnis of Wyeth−Ayerst Research Laboratories for providing access to a 600 MHz Varian Unity Plus spectrometer, and Molecular Simulations Inc. for providing NMRCompass software. Computional facilities at CABM were provided by a grant from the W. M. Keck Foundation.

SUPPORTING INFORMATION AVAILABLE

Table S1, ^{1}H, ^{15}N, and ^{13}C backbone and $^{13}C^{\beta}$ side-chain chemical shifts for wild-type RNase A; Table S2, ^{1}H, ^{15}N, and ^{13}C backbone and $^{13}C^{\beta}$ side-chain chemical shifts for [C65S, C72S] RNase A; Table S3, $^{3}J(H^{N}-H^{\alpha})$ values (Hz) for wild-type and [C65S, C72S] RNase A; Figure S1, 3D ^{15}N-edited PFG NOESY-HSQC pulse sequence; Figure S2, 3D PFG HNCO pulse sequence; Figure S3, 3D PFG HN(CA)CO pulse sequence; Figure S4, 3D PFG HNCA pulse sequence; Figure S5, 3D PFG CA(CO)NH pulse sequence; Figure S6, 3D PFG HA(CA)(CO)NH pulse sequence; Figure S7, 3D PFG HA(CA)NH pulse sequence; Figure S8, 3D PFG CBCA(CO)NH pulse sequence; Figure S9, 3D PFG CBCANH pulse sequence; Figure S10, differences between $^{13}C^{\alpha}$ chemical shift values and statistical coil values ($\Delta\delta C^{\alpha}$) vs amino acid sequence for wild-type and [C65S, C72S] RNase A (26 pages). Ordering information is given on any current masthead page.

REFERENCES

Altmann, K.-H., & Scheraga, H. A. (1990) *J. Am. Chem. Soc. 112*, 4926−4931.

Baldwin, R. L. (1989) *Trends Biochem. Sci. 14*, 291−294.

Beintema, J. J., Schüller, C., Irie, M., & Carsana, A. (1988) *Prog. Biophys. Mol. Biol. 51*, 165 − 192.

Betz, S. F. (1993) *Protein Sci. 2*, 1551−1558.

Blackburn, P., & Moore, S. (1982) *The Enzymes*, pp 317−433, Academic Press, New York.

Buckler, D. R., Haas, E., & Scheraga, H. A. (1995) *Biochemistry 34*, 15965−15978.

Chavez, L. G., Jr., & Scheraga, H. A. (1980) *Biochemistry 19*, 1005−1012.

Chazin, W. J., Kördel, J., Drakenberg, T., Thulin, E., Brodin, P., Grundström, T., & Forsén, S. (1989) *Proc. Natl. Acad. Sci. U.S.A. 86*, 2195−2198.

Clubb, R. T., Thanabal, V., & Wagner, G. (1992) *J. Magn. Reson. 97*, 213−217.

Creighton, T. E. (1986) *Methods Enzymol. 131*, 83−106.

Creighton, T. E. (1988a) *BioEssays 8*, 57−63.

Creighton, T. E. (1988b) *Proc. Natl. Acad. Sci. U.S.A. 85*, 5082−5086.

delCardayré, S. B., Ribó, M., Yokel, E. M., Quirk, D. J., Rutter, W. J., & Raines, R. T. (1995) *Protein Eng. 8*, 261−273.

Dodge, R. W., & Scheraga, H. A. (1996) *Biochemistry 35*, 1548−1559.

Driscoll, P. C., Clore, G. M., Marion, D., Wingfield, P. T., & Gronenborn, A. M. (1990) *Biochemistry 29*, 3542−3556.

Eigenbrot, C., Randal, M., & Kossiakoff, A. A. (1990) *Protein Eng. 3*, 591−598.

Englander, S. W., Downer, N. W., & Teitelbaum, H. (1972) *Annu. Rev. Biochem. 41*, 903−924.

Evans, P. A., Dobson, C. M., Kautz, R. A., Hatfull, G., & Fox. R. O. (1989) *Nature 329*, 266−268.

Feng, W., Ríos, C. B., & Montelione, G. T. (1996) *J. Biomol. NMR 8*, 98−104.

Freund, S. M. V., Wong, K., & Fersht, A. R. (1996) *Proc. Natl. Acad. Sci. U.S.A. 93*, 10600−10603.

Grzesiek, S., & Bax, A. (1992a) *J. Am. Chem. Soc. 114*, 6291−6293.

Grzesiek, S., & Bax, A. (1992b) *J. Magn. Reson. 99*, 201−207.

Hilton, B. D., & Woodward, C. K. (1979) *Biochemistry 18*, 5834−5841.

Hurle, M. R., Eads, C. D., Pearlman, D. A., Seibel, G. L., Thomason, J., Kosen, P. A., Kollman, P., Anderson, S., & Kuntz, I. D. (1992) *Protein Sci. 1*, 91−106.

Hvidt, A., & Nielsen, S. O. (1966) *Adv. Protein Chem. 21*, 287−386.

Jansson, M., Li, Y.−C., Jendeberg, L., Anderson, S., Montelione, G. T., & Nilsson, B. (1996) *J. Biomol. NMR 7*, 131−141.

Jeener, J., Meier, B. H., Bachmann, P., & Ernst, R. R. (1979) *J. Chem. Phys. 71*, 4546−4553.

Kay, L. E., Keifer, P., & Saarinen, T. (1992) *J. Am. Chem. Soc. 114*, 10663−10665.

Konishi, Y., & Scheraga, H. A. (1980a) *Biochemistry 19*, 1308−1316.

Konishi, Y., & Scheraga, H. A. (1980b) *Biochemistry 19*, 1316−1322.

Konishi, Y., Ooi, T., & Scheraga, H. A. (1981) *Biochemistry 20*, 3945−3955.

Konishi, Y., Ooi, T., & Scheraga, H. A. (1982a) *Biochemistry 21*, 4734−4740.

Konishi, Y., Ooi, T., & Scheraga, H. A. (1982b) *Biochemistry 21*, 4741−4748.

Konishi, Y., Ooi, T., & Scheraga, H. A. (1982c) *Proc. Natl. Acad. Sci. U.S.A. 79*, 5734−5738.

Kördel, J., Forsén, S., Drakenberg, T., & Chazin, W. J. (1990) *Biochemistry 29*, 4401−4409.

Kuboniwa, H., Grzesiek, S., Delaglio, F., & Bax, A. (1994) *J. Biomol. NMR 4*, 871−878.

Kumar, A., Ernst, R. R., & Wüthrich, K. (1980) *Biochem. Biophys. Res. Commun. 95*, 1−6.

Laity, J. H., Shimotakahara, S., & Scheraga, H. A. (1993) *Proc. Natl. Acad. Sci. U.S.A. 90*, 615−619.

Laskowski, M. J., & Scheraga, H. A. (1954) *J. Am. Chem. Soc. 76*, 6305−6319.

Li, Y.-J., Rothwarf, D. M., & Scheraga, H. A. (1995) *Nat. Struct. Biol. 2*, 489−494.

Lin, S. H., Konishi, Y., Denton, M. E., & Scheraga, H. A. (1984) *Biochemistry 23*, 5504−5512.

Marion, D., Ikura, M., Tschudin, R., & Bax, A. (1989) *J. Magn. Reson. 85*, 393−399.

Matheson, R. R., Jr., & Scheraga, H. A. (1978) *Macromolecules 11*, 819−829.

Mayr, L. M., Willbold, D., Landt, O., & Schmid, F. X. (1994) *Protein Sci. 3*, 227−239.

Montelione, G. T., & Scheraga, H. A. (1989) *Acc. Chem. Res. 22*, 70−76.

Montelione, G. T., Arnold, E., Meinwald, Y. C., Stimson, E. R., Denton, J. B., Huang, S.-G., Clardy, J., & Scheraga, H. A. (1984) *J. Am. Chem. Soc. 106*, 7946−7958.

Moy, F. J., Seddon, A. P., Campbell, E. B., Böhlen, P., & Powers, R. (1995) *J. Biomol. NMR 6*, 245−254.

Mücke, M., & Schmid, F. X. (1994) *J. Mol. Biol. 239*, 713−725.

Muhandiram, D. R., & Kay, L. E. (1994) *J. Magn. Reson., Ser. B 103*, 203−216.

Naderi, H. M., Thomason, J. F., Borgias, B. A., Anderson, S., James, T. L., & Kuntz, I. D. (1991) *Conformations and Forces in Protein Folding*, pp 86−114, AAA Press, Washington, DC.
Nagayama, K. (1986) *J. Magn. Reson. 69*, 508−510.
Némethy, G., & Scheraga, H. A. (1979) *Proc. Natl. Acad. Sci. U.S.A. 76*, 6050−6054.
Oka, M., Montelione, G. T., & Scheraga, H. A. (1984) *J. Am. Chem. Soc. 106*, 7959−7969.
Pace, N. C., Shirley, B. A., & Thomson, J. A. (1989) in *Protein Structure, A Practical Approach* (Creighton, T. E., Ed.) pp 311−330, IRL Press, New York.
Pardi, A., Billeter, M., & Wüthrich, K. (1984) *J. Mol. Biol. 180*, 741−751.
Privalov, P. L. (1979) *Adv. Protein Chem. 33*, 167−241.
Rico, M., Bruix, M., Santoro, J., Gonzalez, C., Neira, J. L., Nieto, J. L., & Herranz, J. (1989) *Eur. J. Biochem. 183*, 623−638.
Ríos, C. B., Feng, W. F., Tashiro, M., Shang, Z., & Montelione, G. T. (1996) *J. Biomol. NMR*, 345−350.
Robertson, A. D., Purisima, E. O., Eastman, M. A., & Scheraga, H. A. (1989) *Biochemistry 28*, 5930−5938.
Rothwarf, D. M., & Scheraga, H. A. (1991) *J. Am. Chem. Soc. 113*, 6293−6294.
Rothwarf, D. M., & Scheraga, H. A. (1993a) *Biochemistry 32*, 2671−2979.
Rothwarf, D. M., & Scheraga, H. A. (1993b) *Biochemistry 32*, 2680−2689.
Rothwarf, D. M., & Scheraga, H. A. (1993c) *Biochemistry 32*, 2690−2697.
Rothwarf, D. M., & Scheraga, H. A. (1993d) *Biochemistry 32*, 2698−2703.
Santoro, J., Gonzalez, C., Bruix, M., Neira, J. L., Nieto, J. L., Herranz, J., & Rico, M. (1993) *J. Mol. Biol. 229*, 722−734.
Scheraga, H. A., Konishi, Y., & Ooi, T. (1984) *Adv. Biophys. 18*, 21−41.
Scheraga, H. A., Konishi, Y., Rothwarf, D. M., & Mui, P. W. (1987) *Proc. Natl. Acad. Sci. U.S.A. 84*, 5740−5744.
Spera, S., & Bax, A. (1991) *J. Am. Chem. Soc. 113*, 5490−5492.
Staley, J. P., & Kim, P. S. (1992) *Proc. Natl. Acad. Sci. U.S.A. 89*, 1519−1523.
Swadesh, J. K., Montelione, G. T., Thannhauser, T. W., & Scheraga, H. A. (1984) *Proc. Natl. Acad. Sci. U.S.A. 81*, 4606−4610.
Talluri, S., Rothwarf, D. M., & Scheraga, H. A. (1994) *Biochemistry 33*, 10437−10449.
Thanabal, V., Omecinsky, D. O., Reily, M. D., & Cody, W. L. (1994) *J. Biomol. NMR 4*, 47−59.
Udgaonkar, J. B., & Baldwin, R. L. (1990) *Proc. Natl. Acad. Sci. U.S.A. 87*, 8197−8201.
van Mierlo, C. P. M., Darby, N. J., Neuhaus, D., & Creighton, T. E. (1991) *J. Mol. Biol. 222*, 353−371.
Wishart, D. S., Bigam, C. G., Yao, J., Abildgaard, F., Dyson, H. J., Oldfield, E., Markley, J. L., & Sykes, B. D. (1995) *J. Biomol. NMR 6*, 135−140.
Wlodawer, A., Svensson, L. A., Sjölin, L., & Gilliland, G. L. (1988) *Biochemistry 27*, 2705−2717.
Wright, P. E., Dyson, H. J., & Lerner, R. A. (1988) *Biochemistry 27*, 7167−7175.
Xu, X., Rothwarf, D. M., & Scheraga, H. A. (1996) *Biochemistry 35*, 6406−6417.
Zimmerman, D. E., & Montelione, G. T. (1995) *Curr. Opin. Struct. Biol. 5*, 664−673.
Zimmerman, D. E., Kulikowski, C. A., Huang, Y., Feng, W., Tashiro, M., Shimotakahara, S., Powers, R., Chien, C., & Montelione, G. T. (1997) *J. Mol. Biol.* (in press).

BI963024K